

# Micro Holographic Particle Image Velocimetry: Digital 3C3D Measurement of Free Jet Flow

by

H. Yang, N. A. Halliwell and J. M. Coupland

Wolfson School of Mechanical and Manufacturing Engineering

Loughborough University, Loughborough, Leicestershire, LE11 3TU, UK

Email: h.yang@lboro.ac.uk

## ABSTRACT

In this paper, we investigate the potential of holographic particle image velocimetry (HPIV) for instantaneous, three-component (3C) velocity measurements from a three-dimensional (3D) volume within micro-fluidic devices. A transmission microscope utilizing coherent detection is used to make simultaneous holographic recording of micro scale flow. An off-axis reference beam diverges from a (virtual) point that is in the far focal plane of the imaging object lens. In this way, the phase curvature introduced by the imaging process is exactly matched by the curvature of the reference beam, such that straight carrier fringes are observed in the CCD array plane. The carrier modulated intensity distribution can be thought of, therefore, as a holographic recording of the optical field in the object plane of the objective. Demodulating the recorded intensity by Fourier transformation gives the complex amplitude in the object plane of the imaging system and the equation of free-space propagation can be used to reconstruct the field in different planes. The complex amplitude of the light scattered from a given region of the flow is identified and 3D complex amplitude correlation (3DCAC) is used to locate the particle displacement.

The technique is demonstrated using a free jet flow in a microchannel. For the case of sparse seeding, a correlation signal is observed above the background over a cluster of space. In order to assign the measured displacement to a velocity at a particular point in the flow, the method used here is to cluster the measured data into regions identified by high correlation strength. The measured velocity is then ascribed to the geometric centre of this cluster and all other data from the cluster is discarded. Using this approach 137 vectors have been extracted from the 12,800 correlation measurements and are shown in the quiver plot of Figure 1. The vectors that have been simultaneously measured throughout the  $0.5 \times 0.5 \times 0.6 \text{ mm}^3$  volume clearly show behaviour of the jet flow.

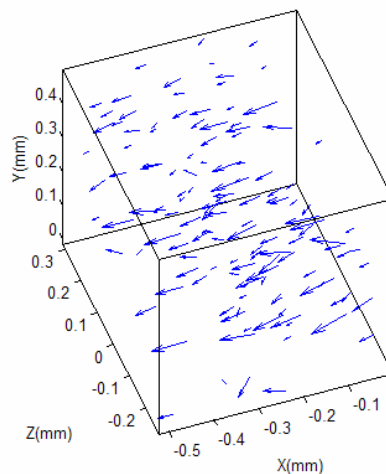


Figure 1 3D velocity map of free jet fluid flow (137 vectors in the size of  $0.5 \times 0.5 \times 0.6 \text{ mm}^3$  volume)

## 1. INTRODUCTION

Micro Particle Image Velocimetry ( $\mu$ PIV) was introduced by Santiago et al. as a means to investigate flow structures within micro-fluidic devices (Santiago et al., 1998). In their work two component velocity measurements were taken from the object plane of a microscope using similar methods to those used in digital particle image velocimetry (DPIV) (Westerweel, 1997). The technique was considered further by Meinhart et al. who analysed numerical aperture (NA) requirement, the need for sparse seeding and ensemble averaged results to ensure that the plane of interest is sufficiently well defined (Meinhart et al., 1999). More recently, some practical applications of  $\mu$ PIV have been described including commercial inkjet printheads (Tretheway et al., 2002) and BioMEMS devices (Santiago, 2001). Currently,  $\mu$ PIV is able to deliver two-component (2C) planar (2D) velocity measurements. For the case of steady flows, a 2C-2D setup has been scanned through the 3D volume and detailed flow maps have been created by averaging.

In parallel efforts, researchers have investigated HPIV as a means to make instantaneous, 3C velocity measurements from a 3D volume of interest (e.g. Coupland and Halliwell, 1993 and Adrian 1991). Unlike scanning PIV, HPIV relies on holography to record and retrieve 3D images of the tracer particles, from which 3C-3D displacements of the particles are extracted. In this paper, we present a variant of HPIV to measure 3C-3D fluid velocity within micro-fluidic devices, which is named micro Holographic Particle Image Velocimetry ( $\mu$ HPIV). As an example, we demonstrate  $\mu$ HPIV for the 3C-3D measurement of a free jet flow in a microchannel.

3D complex amplitude correlation (3DCAC) analysis was originally proposed by Coupland and Halliwell as a means of making 3C-3D velocity measurements, using both the phase and the amplitude information contained within a holographic image. In this way, 3DCAC analysis has been shown to inherently tolerant to aberrations induced by poor quality windows for example (Coupland et al., 1997). In this paper, we demonstrate 3DCAC analysis in  $\mu$ HPIV and show for the first time that this can be accomplished with a standard CCD imaging device in a purely digital environment.

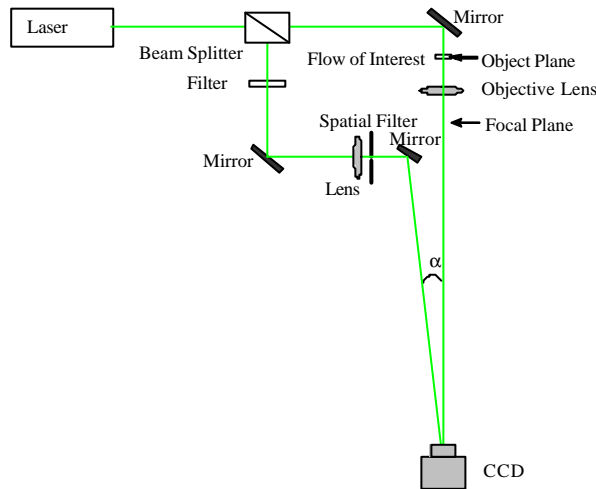


Figure 2 Optical configuration

## 2. THEORY

### 2.1 Recording

Figure 2 illustrates the principle of digital  $\mu$ HPIV. A transmission microscope utilizing coherent detection is used to make simultaneous holographic recording of micro scale flow. According to paraxial imaging theory (e.g. Goodman, 1996), the image complex amplitude  $U_i(x_i, y_i)$  at coordinates  $(x_i, y_i)$  at a distance  $z_i$  behind the lens is given in terms of the object complex amplitude  $U_o(x_o, y_o)$ , such that,

$$U_i(x_i, y_i) = \left[ \frac{1}{M} U_o \left( -\frac{x_i}{M}, -\frac{y_i}{M} \right) \otimes h(x_i, y_i) \right] \exp \left[ j \frac{k}{2z_i} \left( 1 + \frac{1}{M} \right) (x_i^2 + y_i^2) \right] \quad (1)$$

where  $M$  represents the magnification of the system,  $k$  is the wave number,  $\otimes$  denotes convolution and  $h(x_i, y_i)$  is the point-spread function. If the extent of  $h(x_i, y_i)$  is small it can be neglected, in which case the image complex amplitude  $U_i(x_i, y_i)$  of Equation (1) is a magnified version of the object amplitude distribution multiplied by a quadratic phase distribution such that,

$$U_i(x_i, y_i) = U_o \left( -\frac{x_i}{M}, -\frac{y_i}{M} \right) \exp \left[ j \frac{k}{2z_i} \left( 1 + \frac{1}{M} \right) (x_i^2 + y_i^2) \right] \quad (2)$$

In this work we use an off-axis reference beam,  $U_r(x_i, y_i)$ , that diverges from a (virtual) point that is in the far focal plane of the imaging object lens. This is essentially the image of a tilted plane wave in the object plane and as such, the complex amplitude of the reference beam  $U_r(x_i, y_i)$  can be written as

$$U_r(x_i, y_i) = \exp \left\{ j \frac{k}{2z_i} \left( 1 + \frac{1}{M} \right) [(x_i + z_i \sin \alpha)^2 + y_i^2] \right\} \quad (3)$$

where  $\alpha$  is the angle between the reference beam and the object beam (Figure 2). Finally, we have the intensity distribution at the CCD plane  $I(x_i, y_i)$

$$I(x_i, y_i) = |U_r + U_i|^2 = 1 + |U_o|^2 + U_o \left( -\frac{x_i}{M}, -\frac{y_i}{M} \right) \exp(-j2\mathbf{p} \cdot \mathbf{f}_{x_i} x_i) + U_o^* \left( -\frac{x_i}{M}, -\frac{y_i}{M} \right) \exp(j2\mathbf{p} \cdot \mathbf{f}_{x_i} x_i) \quad (4)$$

where  $f_{xi} = (1+1/M)\sin \alpha / \lambda$  is the spatial frequency of the carrier fringes and  $\lambda$  is the wavelength. It can be seen that the phase curvature introduced by the imaging process is exactly matched by the curvature of the reference beam such that straight carrier fringes are observed in the CCD array plane in the absence of any object. In this way, the carrier modulated intensity distribution  $I(x_i, y_i)$  can be thought of as a holographic recording of the optical field in *the object plane of the objective*.

## 2.2 Reconstruction

The first step in the analysis procedure is to demodulate the signal to find the complex amplitude in the object plane of the imaging system. Applying Fourier transformation to the recorded intensity of Equation (4), we have

$$\text{FT}[I(x_i, y_i)] = \delta(0,0) + \text{FT}\left[U_o \left( -\frac{x_i}{M}, -\frac{y_i}{M} \right)\right] \delta(f_x - f_{x_i}, 0) + \text{FT}\left[U_o^* \left( -\frac{x_i}{M}, -\frac{y_i}{M} \right)\right] \delta(f_x + f_{x_i}, 0) \quad (5)$$

where  $\delta$  is a delta function and FT represents Fourier transformation. Isolating the second term of Equation (5), using inverse Fourier transformation and then scaling by the system magnification, gives the optical field in the object plane of the microscope  $U_o(x_o, y_o)$ .

In order to analyse the flow recording it is necessary to decompose the field into parts associated with different regions within the flow. In our previous work, using conventional holography we have used an aperture that is physically placed in the real image (Coupland and Halliwell, 1993). In this study we identify a region of interest or interrogation region within the numerical holographic reconstruction. Since it is usual for the object plane of the imaging system to be some where within the flow field, our initial interrogation regions are areas of the field reconstructed from this plane. In this case, we segment the image into regions of 64x64pixels. Subsequently the field is reconstructed in different planes,  $U_o(x_o, y_o; z)$ , using the free-space propagation equation

$$U_o(x_o, y_o; z) = \text{FT}^{-1} \left\{ \text{FT}[U_o(x_o, y_o)] H(k_x, k_y; z) \right\} \quad (6)$$

where  $H(k_x, k_y; z) = \exp(j2pz\sqrt{l^2 - k_x^2 - k_y^2})$  is the transfer function of the wave propagation and  $FT^{-1}$  denote inverse Fourier transformation. The field is then segmented in the same way and each interrogation region is analysed as follows.

### 2.3 Analysis

Let the complex amplitude of the optical field transmitted by the corresponding to first and second exposure interrogation areas be represented by  $U_1(x, y)$  and  $U_2(x, y)$ . Accordingly,  $U_1(x, y)$  and  $U_2(x, y)$  can be decomposed into its spectrum of plane-wave components  $S_1(k_x, k_y)$  and  $S_2(k_x, k_y)$  respectively defined by the two-dimensional Fourier transformation,

$$S_1(k_x, k_y) = \int_{-\infty}^{+\infty} U_1(x, y) \exp[-2\pi j(k_x x + k_y y)] dx dy \quad (7)$$

$$S_2(k_x, k_y) = \int_{-\infty}^{+\infty} U_2(x, y) \exp[-2\pi j(k_x x + k_y y)] dx dy \quad (8)$$

The cross-spectral density can be calculated from these equations by

$$P_{S_1 S_2}^*(k_x, k_y) = S_1(k_x, k_y) S_2^*(k_x, k_y) \quad (9)$$

As the monochromatic wave vector components  $k_x, k_y$  and  $k_z$  in  $\underline{k}$ -space are interrelated through  $|\underline{k}| = l/?$ ,  $P_{S_1 S_2}^*(k_x, k_y)$ , described by its wave vector components  $k_x$  and  $k_y$  in a plane, can be projected into the surface of the half Ewald sphere (Figure 3) to obtain the 3D power spectrum distribution  $P_{S_1 S_2}(\underline{k})$  in  $\underline{k}$ -space. In practice, the CCD camera only records interference between the shifted wavefronts over a solid angle that is defined by the object space NA of the objective lens (Figure 2). Consequently, the wave vector components in  $\underline{k}$ -space are limited to a region defined by this angle.

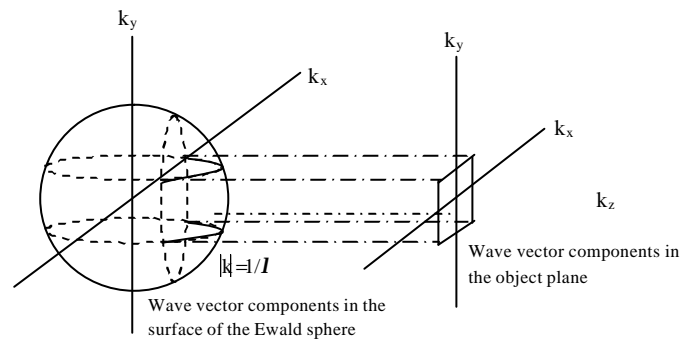


Figure 3 Wave vector mapping

The 3D power spectrum distribution  $P_{S_1 S_2}(\underline{k})$ , written using a wave-vector notation, is given by

$$P_{S_1 S_2}(\underline{k}) = S_1(\underline{k}) S_2^*(\underline{k}) \quad (10)$$

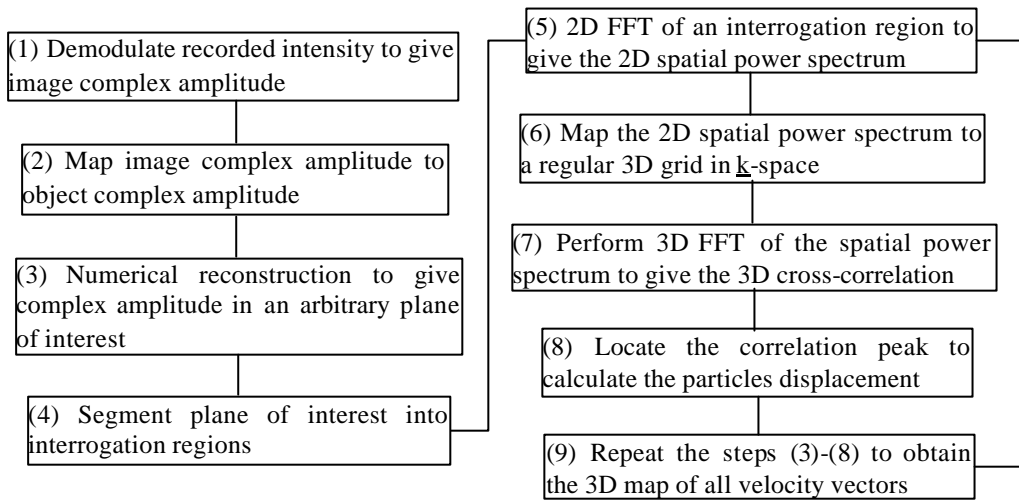
If it is assumed that the particles in the interrogation areas move in unison a distance  $\underline{s}$ , the second exposure field  $U_2(\underline{r})$  is identical to the first exposure field  $U_1(\underline{r})$  but shifted by  $\underline{s}$ . The 3D cross-correlation of two

interrogation areas  $\mathbf{R}_{s_1, s_2}(\mathbf{r})$  can be calculated by the 3D inverse Fourier transformation of the 3D cross-spectral density  $\mathbf{P}_{s_1, s_2}(\mathbf{k})$ . We have the 3D complex cross-correlation (Yang et al., 2003)

$$\mathbf{R}_{s_1, s_2}(\mathbf{r}) = \mathbf{R}_1(\mathbf{r}) * \exp(-i\mathbf{j} \cdot \mathbf{r}) \delta(\mathbf{r} - \mathbf{s}) \quad (11)$$

where  $\mathbf{R}_1(\mathbf{r})$  is the auto-correlation of the optical field transmitted by the first interrogation area,  $\phi$  is a constant and  $\delta$  is the Dirac delta function. The intensity distribution in the output space of the 3D cross-correlation consists of one dominant peak that is situated at positions equal to the particle displacement. In this way, the three components of the particle image displacement can be found by searching the correlation field for the brightest point. The particle velocity is finally obtained by dividing the displacement by the time interval between the two recordings. This process is repeated at each interrogation area within the optical field, resulting in a 3D map of velocity vectors to describe the flow.

A computer program written in MatLab was used to calculate the particles displacement. The algorithm proceeds as follows:



### 3. EXPERIMENTAL SETUP and RESULTS

The experimental configuration shown in figure 2 was used to make simultaneous holographic recording of the jet flow inside the micro-channel. The system NA is restricted by the objective lens to 0.25 ( $f\#=2$ ) and the system magnification  $M$  is 14. The CCD array of 1280x1024pixels and pixel size of  $6.8\mu\text{m} \times 6.8\mu\text{m}$  operating at 3fps is used to record a sequence of holograms and accordingly the field of view (corresponding to the size of the field in the object plane) was approximately  $600\mu\text{m} \times 500\mu\text{m}$ . As the maximum fringe frequency of the interference pattern which can be resolved by the CCD camera array is the inverse of twice the pixel size, this gives a maximum reference beam angle,  $\alpha$ , of about  $2.5^\circ$ .

The analysis of each sequential pair of particulate holograms is as described above. The optical field is reconstructed in 20 planes separated by  $30\mu\text{m}$ . Subsequently, the particle velocity is performed using 3D complex cross-correlation technique on each  $64 \times 64$ pixels ( $30\mu\text{m} \times 30\mu\text{m}$ ) area of this field (with 50% overlap). In all, 12,800 cross-correlations were calculated in this way from each pair of holographic images.

In our experiments to date, we have considered relatively sparsely seeded flow using  $5\mu\text{m}$  hollow glass micro-spheres and this has illustrated some of the attributes of the analysis procedure. For the case of sparse seeding, it is noted that a correlation signal is observed above the background (stationary noise caused by scattering from windows etc.) over a cluster of space. This is most noticeable in the depth direction. Figure 4 displays the correlation signals of the corresponding interrogation regions at different  $z$  position of (a) 0mm, (b) -0.12mm and (c) -0.24mm, respectively. To illustrate the process, the centre pixel is highlighted to

show zero displacement. Figure 4 shows the magnitude of the cross-correlation peak as a function of depth-ordinate,  $z$ . This makes it possible to distinguish particles depth from the correlation signal peaks. The profile of correlation signal becomes wider and the peak of correlation signal becomes smaller if the particle becomes more out-of-focus. In the case shown in Figure 5, it can be seen that the signal could be attributed to one particle located approximately 0.12mm from the object plane of the microscope.

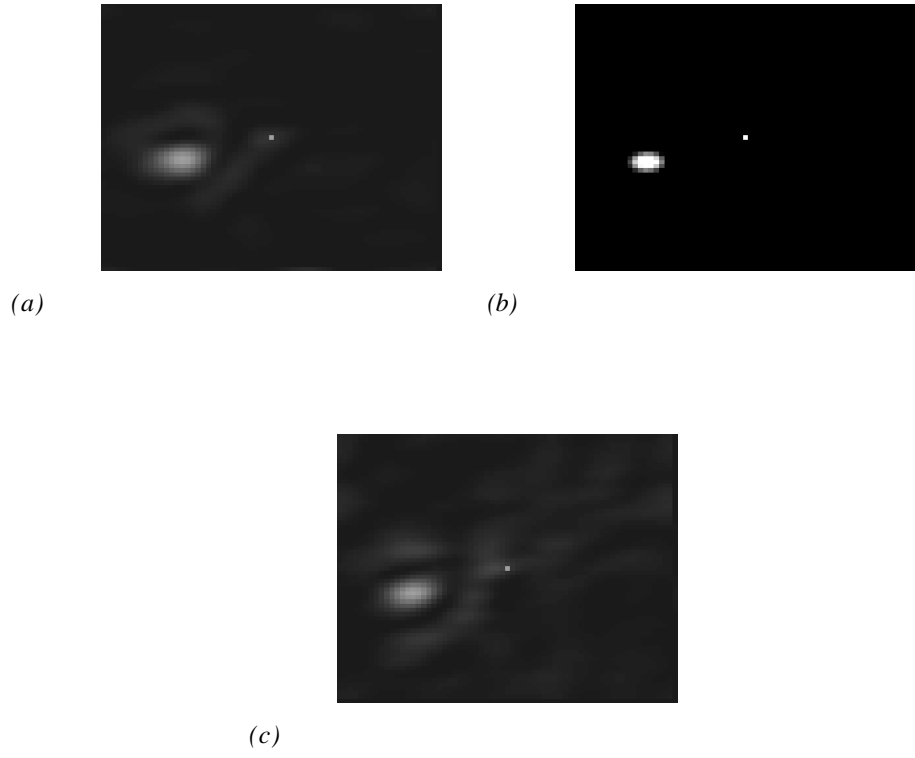


Figure 4 The correlation signal of the corresponding interrogation regions at different  $z$  position of (a) 0mm, (b) -0.12mm and (c) -0.24mm, respectively (the centre pixel is a zero velocity reference).

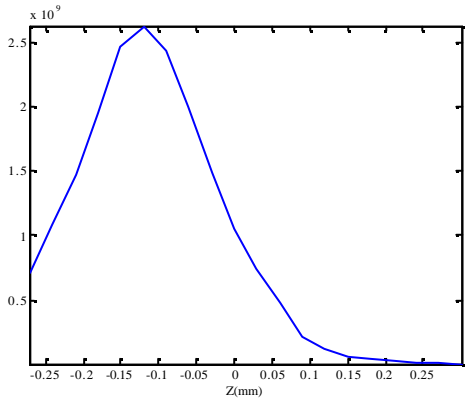


Figure 5 Correlation peaks throughout the  $z$ -direction in the flow volume.

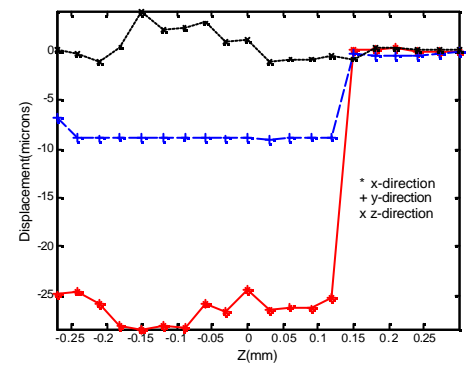


Figure 6 The calculated three-component displacement vectors from the correlation peaks position throughout the depth-direction of the flow volume

Figure 6 shows the corresponding 3C particle displacement vectors that have been extracted from the correlation peak position of Figure 5. It can be deduced that the displacement of this particle is approximately  $\Delta x=-28.38\mu\text{m}$ ,  $\Delta y=-9.02\mu\text{m}$  and  $\Delta z=4.12\mu\text{m}$  and these measurements are reasonably consistent over the space defined by the width of the peak in Figure 5.

It is clear from the results that some method is needed to assign the measured displacement to a velocity at a particular point in the flow. As the seeding concentration is increased, there could be a number of peaks in each correlation. These peaks correspond to the movement of particles that are both in and out-of-focus. However, the largest correlation peak is expected to correspond to the brightest particle image. A suitable method is needed to locate this in 3D space. The method used here is to cluster the measured data into regions identified by high correlation strength. The measured velocity is then ascribed to the geometric centre of this cluster and all other data from the cluster is discarded. Figure 7 (a) and (b) shows the in-plane two components velocity map in the image plane before and after the measurement data is identified, respectively. Using this approach 137 vectors have been extracted from the 12,800 correlation measurements and are shown in the quiver plot of figure 8. The vectors that have been simultaneously measured throughout the  $0.5\times 0.5\times 0.6\text{mm}^3$  volume clearly show behaviour of the jet flow.

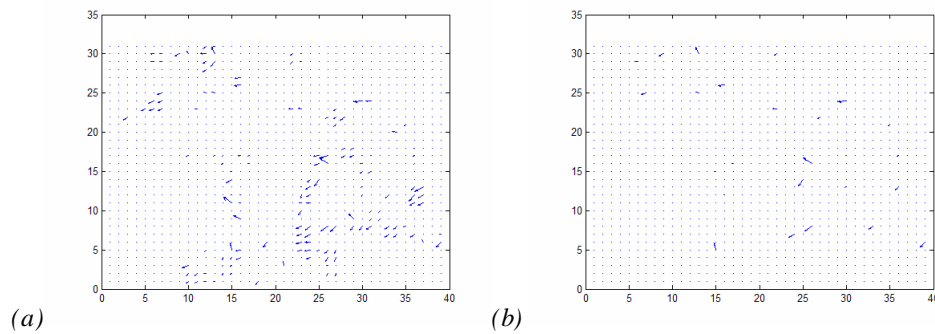


Figure 7 The in-plane two components velocity map in the image plane (a) before and (b) after the measurement data is identified

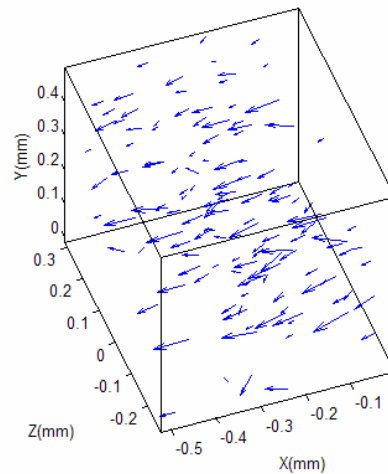


Figure 8 3D velocity map of free jet fluid flow (137 vectors in the size of  $0.5\times 0.5\times 0.6\text{mm}^3$  volume)

#### 4. CONCLUSION

In this paper,  $\mu\text{HPIV}$  has been demonstrated as a means to make 3C-3D measurements in micro-fluidics. For the case of sparse seeding, 3D complex correlation methods and cluster analysis has provided high

resolution ( $<1\mu\text{m}$ ) data on a  $30\mu\text{m}$ , 3D grid. Clearly, more work is necessary to prove the accuracy of the technique and to ascertain how many vectors can be extracted in this way from a more densely seeded flow.

## REFERENCES

- Adrian, R. J. (1991), "Particle-imaging techniques for experimental fluid mechanics", *Ann. Rev. Fluid Mech.*, 23, p261-304
- Coupland, J. M. and Halliwell, N. A. (1993), "Particle image velocimetry: three-dimensional fluid velocity measurement using holographic recording and optical correlation", *Applied Optic*, 131 (8), p1005-1007
- Coupland, J. M. and Halliwell, N. A. (1997), "Holographic Displacement Measurements in Fluid and Solid Mechanics: Immunity to Aberrations by Optical Correlation", *Processing, Proc. R. Soc. A*, 453, p1053-1066
- Goodman, J. W., Introduction to Fourier Optics. Second ed. 1996, New York: McGraw-Hill
- Meinhart, C. D., Wereley, S. T. and Santiago, J. G. (1999), "PIV measurement of a micro-channel flow", *Experiment in Fluids* 27, p414-419
- Santiago, J. G., Wereley, S. T., Meinhart, C. D., D. J. Beebe and Adrian, R. J. (1998), "A particle image velocimetry system for micro-fluidics", *Experiment in Fluids*, 25, p316-319J. Westerweel (1997), "Fundamentals of digital particle image velocimetry", *Measurement of Science and Technology*, 8, p1379-1392
- Santiago, J. G. (2001), "Electroosmotic flows in microchannels with finite inertial and pressure forces", *Anal. Chem*, 73, p2353-2365
- Tretheway, D. and Meinhart, C. D. (2002), "Fluid slip near hydrophobic microchannel wall", *Phys. of Fluids*, 14(3), L9-L12
- Yang, H., Halliwell, N. A. and Coupland, J. M. (2003), "Digital shearing method for three-dimensional data extraction in HPIV", *Applied Optic*, 42(8), p6458-6465R. J. Adrian (1991), "Particle-imaging techniques for experimental fluid mechanics", *Ann. Rev. Fluid Mech.*, 23, p261-304